

# Role of Nitrogen Dioxide in the Production of Sulfate during Chinese Haze-Aerosol Episodes

Lijie Li, Michael R. Hoffmann, and Agustín J. Colussi\*

Department of Environmental Science & Engineering, California Institute of Technology, Pasadena, California 91125, United States

Supporting Information

ABSTRACT: Haze events in China megacities involve the rapid oxidation of SO<sub>2</sub> to sulfate aerosol. Given the weak photochemistry that takes place in these optically thick hazes, it has been hypothesized that SO2 is mostly oxidized by  $NO_2$  emissions in the bulk of pH > 5.5 aerosols. Because  $NO_2(g)$  dissolution in water is very slow and aerosols are more acidic, we decided to test such a hypothesis. Herein, we report that > 95% of  $NO_2(g)$  disproportionates  $[2NO_2(g) + H_2O(1) = H^+ + NO_3^-(aq) + HONO (R1)]$  upon hitting the surface of NaHSO<sub>3</sub> aqueous microjets for  $< 50 \mu s$ , thereby giving rise to strong  $NO_3^-$  (m/z 62) signals detected by online electrospray mass spectrometry, rather than oxidizing  $HSO_3^-$  (m/z 81) to  $HSO_4^-$  (m/z 97) in the relevant pH 3-6 range. Because NO<sub>2</sub>(g) will be consumed via R1 on the surface of typical aerosols, the oxidation of S(IV) may in fact be driven by the HONO/NO<sub>2</sub> generated therein. S(IV) heterogeneous oxidation rates are expected to



primarily depend on the surface density and liquid water content of the aerosol, which are enhanced by fine aerosol and high humidity. Whether aerosol acidity affects the oxidation of S(IV) by HONO/NO<sub>2</sub><sup>-</sup> remains to be elucidated.

# 1. INTRODUCTION

Chinese megacities often experience haze events  $(HEs)^{1-7}$  that severely impair visibility and induce acute health effects. 5,6,8-1 Hazes mainly consist of sulfate aerosols produced in the atmospheric processing of SO<sub>2</sub> and NO<sub>2</sub> emissions under particularly adverse meteorological conditions. 12-14 Current models of chemistry in HEs significantly underestimate sulfate formation, revealing that the mechanism of SO<sub>2</sub> oxidation is not well understood. 15-17 The drastic attenuation of actinic radiation in hazes<sup>18-21</sup> suggests that SO<sub>2</sub> is oxidized by  $NO_2(g)$  via heterogeneous processes on the aerosol itself, rather than by photogenerated oxidants in the gas-phase. The details of such a process are uncertain.

Known SO<sub>2</sub> atmospheric oxidation pathways include gas phase reactions with OH radicals and stabilized Criegee intermediates and aqueous phase reactions with  $O_3^{22}$   $H_2O_2$ organic peroxides, and NO<sub>x1</sub> as well as autoxidation catalyzed by transition metal ions. The low concentrations of photogenerated oxidants 18,23-30 imply that the chemistries of SO<sub>2</sub> and NO2 in HEs are intertwined. These observations have led to a hypothesis that HSO<sub>3</sub><sup>-</sup>(aq) is rapidly oxidized by the NO<sub>2</sub>(g) dissolved in aqueous aerosol phases assumed to be at pH > 5.5 (reaction R0):

$$2NO_2(aq) + HSO_3^-(aq) + H_2O(l) = 2H^+(aq)$$
  
+  $HSO_4^-(aq) + 2NO_2^-(aq)$  (R0)

on the basis of R0 rates measured in bulk water.31-33 Good agreement between field observations and model results on sulfate-aerosol formation in HEs could be obtained by assuming that R0 proceeds on the surface pH >5.5 aqueous aerosols at the rates previously reported at pH ~ 6 in bulk water.31-34 However, the assumptions that aerosols are at pH >5.5 and NO<sub>2</sub>(g) dissolves in large surface-to-volume aerosol droplets as NO<sub>2</sub>(aq) as it does in bulk water may not apply.<sup>35–45</sup> Most recent studies suggest that HE aerosols are in fact in the pH 3–5 range.<sup>46–52</sup> Previous laboratory experiments have shown that collisions of NO<sub>2</sub>(g) at parts per million level (i.e., in the absence of  $N_2O_4$ ) with the surface of aqueous electrolyte solutions (but not on the surface of pure water) yield NO<sub>3</sub>-(aq) via a first-order in [NO<sub>2</sub>] hydrolytic disproportionation catalyzed by anions (reaction R1). 42,45

$$2NO_2(g) + H_2O(1) = H^+ + NO_3^-(aq) + HONO$$
 (R1)

The fact that NO<sub>2</sub>(g) is weakly soluble in pure water (Henry's law constant  $H \sim 0.01~{\rm M~atm^{-1}})$  and its uptake coefficient on pure water is very small  $(\gamma \sim 1 \times 10^{-7})^{53}$  the dissolution of NO<sub>2</sub>(g) in pure water is unfavorable for both kinetic and thermodynamic reasons. The aqueous phase of most atmospheric aerosols, however, is not pure water. In 2009, we found that anions greatly enhance  $NO_2(g)$  uptake on water. The rate-determining step involves the capture of NO<sub>2</sub>(g) by anions X<sup>-</sup> as X-NO<sub>2</sub><sup>-</sup> at air-aqueous interfaces, 42,45 followed by the reaction of  $X-NO_2^-$  with a second  $NO_2(g)$ . This phenomenon accounts for the outstanding discrepancy (by a

October 11, 2017 Received: Revised: January 12, 2018 Accepted: January 29, 2018 Published: January 29, 2018

factor of  $\sim 10^{3-4}$ ) between the  $NO_2(g)$  uptake coefficients measured in neat water <sup>41,53</sup> and those determined on NaCl-seeded droplets in a cloud chamber. <sup>35,39,54</sup> Because HE aerosols naturally contain organic and inorganic anions, the expectation was that the fate of  $NO_2(g)$  would be determined by reaction R1 at actual aerosol air—aqueous interfaces.

Given the societal and economic impact of HEs, we deemed it important to elucidate the actual role of NO<sub>2</sub>(g) in the production of sulfate aerosol under relevant conditions. Herein, we describe experiments in which aqueous 1 mM NaHSO<sub>3</sub> microjets (containing 3 mM EDTA to inhibit the autoxidation of HSO<sub>3</sub><sup>-</sup> catalyzed by pervasive transition metal ions) ejected from a stainless steel syringe are exposed to 5 ppm of NO<sub>2</sub>(g) for  $\leq 50 \ \mu s$  in 1 atm of  $N_2(g)$  at 298 K. Reactant and product ions formed on the outermost water layers of the liquid microjets are detected within 1 ms by online electrospray ionization mass spectrometry (o-ESI-MS). This technique has been used in our laboratory to investigate a suite of gas-liquid reactions at the air-water interface. 55-61 The analysis of our experimental results focuses on the fate of NO2(g), and the competition between reactions R0 and R1 during collisions of NO<sub>2</sub>(g) with the surface of aqueous HSO<sub>3</sub><sup>-</sup> solutions under conditions relevant to HEs. To the best of our knowledge, this is the first study to provide direct experimental evidence of the extent of S(IV) oxidation by  $NO_2(g)$  on the surface of aqueous electrolyte solutions over a wide pH range.

## 2. METHODS

Reactive interactions of  $NO_2(g)$  with  $HSO_3^-(aq)$  are investigated on the fresh surface of continuously flowing  $HSO_3^-(aq)$  microjets that are crossed by  $NO_2(g)/N_2(g)$  beams in the spray chamber of an electrospray ionization (ESI) mass spectrometer maintained at 1 atm of  $N_2(g)$  and 298 K (Agilent 1100 Series G2445A Ion Trap LC-MS-MSD instrument) (Figure 1). This experimental setup has been described in more

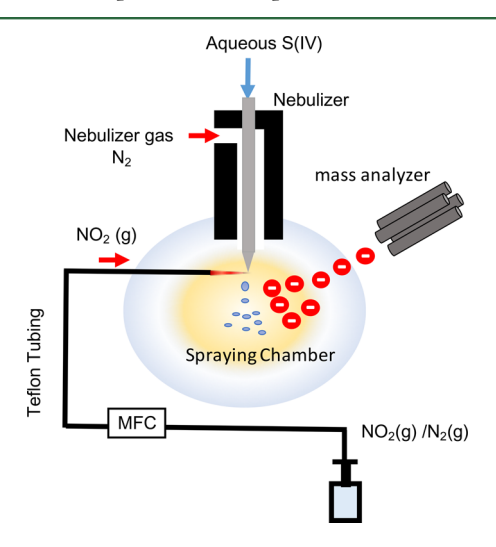


**Figure 1.** Schematic diagram of the experimental setup. MFC is the mass flow controller.

detail in previous reports from our laboratory.  $^{44,45,55,57,58,60-64}$  Aqueous 1 mM NaSO<sub>3</sub>H solutions (containing 3 mM EDTA to chelate pervasive traces of transition metal ions known to catalyze  $HSO_3^-$  autoxidation) are pumped at a rate of 50  $\mu$ L min<sup>-1</sup> through an electrically grounded stainless steel needle injector (100  $\mu$ m bore). These liquid microjets are intersected

by beams of  $NO_2(g)$  diluted in  $N_2(g)$  at controlled flow rates (MKS). Gas-liquid encounters take place during  $\tau \leq 50 \ \mu s$ contact times, which correspond to the estimated lifetimes of the intact microjets prior to their breakup by the nebulizing gas. The outermost layers of the liquid microjets issuing (at 11 cm s<sup>-1</sup>) from the tip of the syringe are pneumatically stripped and nebulized into charged microdroplets by  $N_2(g)$  flowing at a rate of >250 m s<sup>-1</sup> through a coaxial sheath. Anions contained in the charged microdroplets are detected by online ESI mass spectrometry in the m/z 50–100 range. Anion detection was optimized by setting the drying gas temperature to 325 °C and the capillary voltage to 3250 V. Fresh solutions were prepared with Milli-Q water (18.2 M $\Omega$  cm at 25 °C) that had been sparged with N<sub>2</sub>(g) for 8 h to remove dissolved O<sub>2</sub> (except as indicated) within 5 min prior to injection, in a glovebox at < 1 ppm O<sub>2</sub>(g). The pH of solutions was adjusted by adding NaOH(aq) or HCl(aq) and measured with a calibrated pHmeter. Throughout, reported pH values correspond to those measured in the bulk of solutions. A sodium bisulfite solution [40% (w/w), Sigma-Aldrich], hydrochloric acid [>30% (w/w), Sigma-Aldrich], sodium hydroxide (≥ 99.0%, Sigma-Aldrich), ethylenediaminetetraacetic acid (EDTA, > 99.0%, Sigma-Aldrich), and  $48.75 \pm 2$  ppm of  $NO_2(g)$  in  $N_2(g)$  (Airgas) were used as received. The actual  $NO_2(g)$  concentration at the surface of the aqueous microjets is 10 times lower (5 ppm) because of dilution by the nebulizer gas.

## 3. RESULTS

**3.1.** HSO<sub>3</sub><sup>-</sup> Mass Spectral Intensities on Aqueous Surfaces. HSO<sub>3</sub><sup>-</sup> m/z 81 mass spectral signal intensities ( $I_{81}$  values, normalized to their maximum value,  $I_{81,\max}$ ) measured by o-ESI-MS at the gas—aqueous interface of 1 mM NaHSO<sub>3</sub> aqueous microjets as a function of bulk pH are shown as blue data points in Figure 2. The red trace corresponds to [HSO<sub>3</sub><sup>-</sup>]/

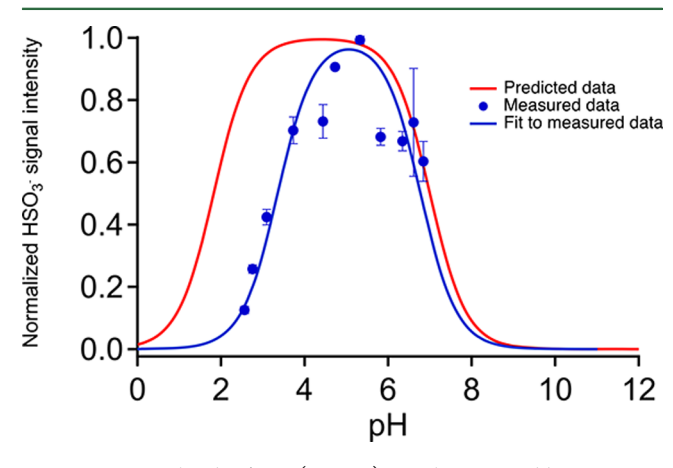


**Figure 2.** Normalized m/z 81 (HSO $_3^-$ ) signals measured by o-ESI-MS on the surface of 1 mM NaHSO $_3$ (aq) microjets as a function of bulk pH (blue symbols and line). HSO $_3^-$  mole fractions calculated from a p $K_{a1}$  (H $_2$ O·SO $_2$   $\rightleftharpoons$  HSO $_3^-$  + H $^+$ ) of 1.8 and a p $K_{a2}$  (HSO $_3^ \rightleftharpoons$  SO $_3^{2-}$  + H $^+$ ) of 7.2 in bulk water (red line).

[HSO<sub>3</sub><sup>-</sup>]<sub>max</sub> values calculated from reported acidity constants in bulk water:  $pK_{a1}$  (H<sub>2</sub>O·SO<sub>2</sub>  $\rightleftharpoons$  HSO<sub>3</sub><sup>-</sup> + H<sup>+</sup>) = 1.8, and  $pK_{a2}$  (HSO<sub>3</sub><sup>-</sup>  $\rightleftharpoons$  SO<sub>3</sub><sup>2-</sup> + H<sup>+</sup>) = 7.2. Experimental mass spectral data clearly display HSO<sub>3</sub><sup>-</sup> deficits at pH < 5 relative to calculated values, which are due to losses of SO<sub>2</sub> to the gas phase. This is considered a feature particular to the HSO<sub>3</sub><sup>-</sup>/SO<sub>2</sub> system because the titration curves of less volatile acids and bases

determined in this setup were in accordance with bulk  $pK_a$  values. The experimental  $HSO_3^-$  signal intensity versus pH data of Figure 2 provide the reference for analyzing the extent of S(IV) oxidation in the following sections.

3.2. NO<sub>2</sub>(g) Reactions on Aqueous Electrolyte Surfaces. Mass spectra acquired before and during exposure of pH  $\sim 5$  (1 mM HSO<sub>3</sub><sup>-</sup> and 3 mM EDTA) aqueous microjets to 5 ppm of NO<sub>2</sub>(g) for  $\leq 50~\mu s$  are shown in Figure 3. The main feature is the appearance of a strong NO<sub>3</sub><sup>-</sup> m/z 62

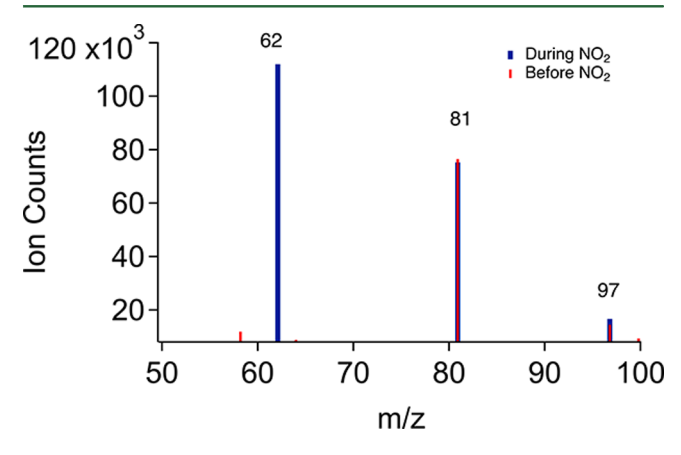


**Figure 3.** ESI mass spectra of the surface of aqueous 1 mM NaHSO<sub>3</sub> and 3 mM EDTA, pH  $\sim$  5 microjets before and after exposure to 5 ppm of NO<sub>2</sub>(g). Note the presence of minor HSO<sub>4</sub><sup>-</sup> (m/z 97) impurities in the initial solutions.

signal, in contrast with the minimal variations displayed by both  $HSO_3^-$  m/z 81 and  $HSO_4^-$  m/z 97 signals upon exposure to  $NO_2(g)$ . This outcome means that  $NO_2(g)$  molecules hitting the surface of pH  $\sim 5$   $HSO_3^-$  microjets mainly undergo fast (within 50  $\mu$ s) disproportionation, leaving barely any  $NO_2$  for diffusing into the bulk liquid, and supposedly participate in reaction R0. The following section explores the effect of pH on the competition between reactions R0 and R1.

**3.3.** Oxidation of S(IV) on Aqueous Surfaces. The extent of  $HSO_3^-(aq)$  oxidation by  $NO_2(g)$ , expressed by the ratio of  $[HSO_3^-]/[HSO_4^-] \propto I_{81}/I_{97}$  signal intensities, as a function of pH is shown in Figure 4.  $I_{81}$  values correspond to measured  $I_{81}$  signals corrected for the depressing effect of the  $NO_3^-$  simultaneously produced via reaction R1 at the air–aqueous interface (see below). Figure 4 clearly shows that the extent of  $HSO_3^-(aq)$  oxidation via reaction R0 is minimal throughout, barely exceeding the experimental error in the pH 3–6 range that is relevant to HEs.

We quantified the fraction of  $NO_2(g)$  that oxidizes  $HSO_3^-(aq)$  at the air—aqueous interface as  $f_{RO}$ , defined by eq E1. In eq E1,  $\Delta_{81}'$  is calculated from the decrease in the measured  $I_{81}$  signals,  $\Delta_{81}$ , corrected for the  $NO_3^-$  depressing effect mentioned above, which is further multiplied by the ratio  $\beta$  ( $I_{62}/I_{82}$ ) of the o-ESI mass spectra measured in 1 mM  $HSO_3^-/1$  mM  $NO_3^-$  equimolar solutions at each pH to convert  $I_{81}$  decrements into equivalent  $\Delta_{62}$   $NO_3^-$  changes.

$$f_{\rm R0} = \frac{\Delta_{81}'}{\Delta_{81}' + \Delta_{62}} \tag{E1}$$

We found that  $f_{R0}$  increases from < 6% within the pH range of 3.0–6.0 to 42% at pH 10.8. It also increases with acidity to 16% at pH 2.5 (Figure 5). This finding means that the anion-catalyzed hydrolytic disproportionation of  $NO_2(g)$  on aquated

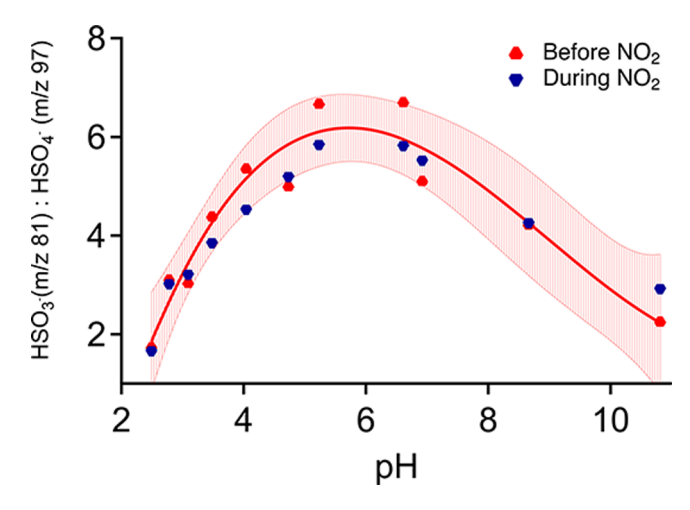


**Figure 4.** Red symbols, the red line, and the 95% confidence band correspond to the ratio of  $HSO_3^-/HSO_4^ I_{81}/I_{97}$  signal intensities on the surface of 1 mM NaHSO<sub>3</sub> and 3 mM EDTA microjets in  $N_2(g)$ -sparged MQ water as a function of bulk pH. Blue symbols represent data after exposure to 5 ppm of  $NO_2(g)$  for < 50  $\mu$ s.

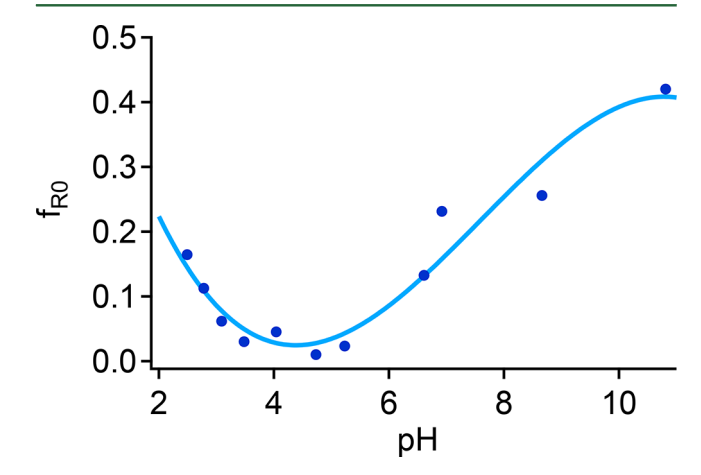


**Figure 5.** Fraction of NO<sub>2</sub>(g) that contributes to S(IV) oxidation,  $f_{R0}$  (eq E1), as a function of pH.

aerosol surfaces (reaction R1) will outcompete reaction R0 throughout, particularly under atmospherically relevant acidic conditions. 35,39,41,43,45,57 We have shown that most electrolytes increase the uptake coefficient of  $NO_2(g)$  from  $\gamma < 1.0 \times 10^{-7}$ in pure water<sup>37</sup> to  $\gamma$  in the  $10^{-3}$ – $10^{-4}$  range at air–aqueous electrolyte interfaces.<sup>35,39,41,45,57</sup> The mechanism of enhancement involves trapping NO<sub>2</sub>(g) by X<sup>-</sup> as X-NO<sub>2</sub><sup>-</sup> at the airwater interface, which can react further with  $NO_2(g)$ .<sup>45</sup> This interfacial process is expected to dominate the fate of  $NO_2(g)$ during HEs due to the large surface-to-volume ratio of aerosol microdroplets. We have previously shown that the decay of NO<sub>2</sub>(g) on aqueous aerosols via reaction R1 accounts for the similar  $\sim 4$  h NO<sub>2</sub>(g) decay half-lives measured by satellite sightings of urban plumes over world megacities ranging from Singapore to Moscow. 42 We pointed out that if, as generally assumed, NO2(g) were removed by gas phase OH radicals via the  $NO_2(g) + {}^{\bullet}OH(g) = HNO_3(g)$  reaction, much longer decay half-lives would have been observed in winter and at high latitudes, given that "OH radicals follow the sun".69

Next, we performed experiments in which we analyzed, within 5 min via o-ESI-MS, freshly prepared HSO<sub>3</sub><sup>-</sup> solutions in air-saturated water without added EDTA. We detected

 $SO_3^{\bullet-}$  m/z 80 signals whose intensities increase linearly with pH (Figure S3). The formation of  $SO_3^{\bullet-}$  is ascribed to the autoxidation of  $HSO_3^-$  catalyzed by the omnipresent traces of transition metal ions in our solutions. Whether this process makes a significant contribution to the oxidation of S(IV) under HE conditions is the subject of other studies. Additional experiments performed by exposing such  $HSO_3^-$  solutions (in air-saturated deionized water without added EDTA) to  $NO_2(g)$  (Figure S4) led to  $I_{81}/I_{97}$  ratios similar to those depicted in Figure 4 for  $NO_2(g)$ , meaning that  $NO_2$  makes negligible contributions to S(IV) autoxidation in our  $SO_2$  time frames.

#### 4. DISCUSSION

## 4.1. Indirect Role of NO<sub>2</sub>(g) in the Oxidation of S(IV).

Our findings open up new perspectives on the mechanism of S(IV) oxidation by  $NO_2(g)$  during HEs. They underscore the fact that the stoichiometry of reaction R0 could not account for the formation of  $NO_3^-$  in HEs,  $^{32,33}$  because if  $NO_2(g)$  were the only available oxidant and were consumed in reaction R0,  $N(IV)O_2$  could not be oxidized to  $N(V)O_3^-$ . Any valid mechanism should explain (1) how both  $S(IV)O_2$  and  $N(IV)O_2$  are oxidized to  $HS(VI)O_4^-$  and  $N(V)O_3^-$  and (2) how HONO is produced.

We analyzed the fate of  $NO_2(g)$  by considering its reactive uptake on the aerosol via reaction R1 and its photolysis by scattered solar radiation via reaction R2 under representative HE conditions.

$$NO_2(g) + h\nu \ (\lambda \le 420 \text{ nm}) = O(^3P) + NO$$
 (R2)

Rate constants for the reactive uptake of  $NO_2(g)$ ,  $k_{R1}$ , were estimated with eq E2 from the kinetic theory of gases.

$$k_{\rm RI} = \frac{1}{4} \gamma \nu_{\rm NO_2} (S/V) \tag{E2}$$

where  $v_{\rm NO_2}$  (=  $3.7 \times 10^2$  m s<sup>-1</sup>) is the mean thermal speed of NO<sub>2</sub>(g) at 298 K,  $\gamma$  (=  $10^{-3}$ – $10^{-4}$ ) is the estimated range of the reactive uptake coefficient of NO<sub>2</sub>(g) on the surface of aqueous electrolyte solutions,<sup>45</sup> and S/V (in square micrometers per cubic meter) is the surface density of aerosols. Aerosols consist of submicrometer particles with S/V values of  $\lesssim 2 \times 10^{-3}$  m<sup>-1</sup> during hazy days and values that are  $\sim 5$  times smaller on clear days.<sup>33</sup> By assuming that  $\gamma = 10^{-3}$  and  $S/V = 2 \times 10^{-3}$  and  $4 \times 10^{-4}$  m<sup>-1</sup>, we estimate  $k_{\rm R1} \sim 2 \times 10^{-4}$  s<sup>-1</sup> and  $k_{\rm R1} \sim 4 \times 10^{-5}$  s<sup>-1</sup> on hazy and clear days, respectively.

The low O<sub>3</sub>(g) concentrations measured during HEs indicate that the rate of photolysis of NO<sub>2</sub>(g), which generates the  $O(^{3}P)$  atoms involved in  $O_{3}(g)$  formation  $[O_{2} + O(^{3}P) + M =$ O<sub>3</sub> + M], is greatly reduced because of the severe attenuation of actinic sunlight during HEs. We estimated time- and spaceaveraged photolysis rate constants,  $k_{R2}$ , by using the National Center for Atmospheric Research Tropospheric Ultraviolet Visible (TUV) Radiation Model with environmental parameters within the ranges reported for aerosol optical properties and aerosol radiative forcing parameters (see Figure S3).<sup>24,25</sup> Our estimates  $[(k_{R1})_h/(k_{R2})_h^2 \sim 0.5-1.2$ , and  $(k_{R1})_c/(k_{R2})_c \sim 0.01-0.1$  (h, hazy; c, clear)] are semiquantitatively consistent with the premise outlined above and illustrate how the competition between reactions R1 and R2 shifts from hazy to clear days (see Figure S3). However, we suggest that TUV calculations on the competition between reactions R1 and R2 provide a lower bound to  $(k_{R1})_h/(k_{R2})_h$ , because NO<sub>2</sub>(g) is not expected to be uniformly distributed but to accumulate in the

lower layers of dense hazes, where there is minimal actinic radiation and photochemical activity.

Together, our estimates and experimental results support the view that the leading pathway for  $NO_2(g)$  during HEs is its heterogeneous disproportionation into  $NO_3^- + HONO/NO_2^- + H^+$  via reaction R1. Note that reaction R1 is autocatalytic because it ultimately contributes to the increases in the mass and S/V of the aerosols on which it takes place. The rapid development of HEs is in fact consistent with such an autocatalytic process. The fact that relative humidity increments are tracked by increased particle number concentrations and surface area density S/V (square micrometers per cubic meter) of  $PM_{2.5}$ , particularly in the accumulation mode, also supports the notion that the liquid particles present under such conditions grow from autocatalytic heterogeneous processes.<sup>71</sup>

Reaction R1 accounts for the direct formation of NO<sub>3</sub><sup>-</sup> and HONO and would also account for the formation of HSO<sub>4</sub><sup>-</sup> if the HONO/NO<sub>2</sub><sup>-</sup> produced in reaction R1 could ultimately oxidize S(IV) (see Figure 6).<sup>72–78</sup> As a result, because  $f_{R0} \le 0.1$ 

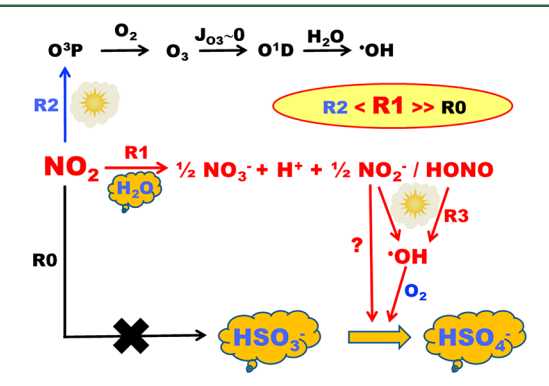


Figure 6.  $NO_2$  reactions and their impact on S(IV) oxidation during haze-aerosol events.

in the realistic pH range of 3-6, i.e., nearly independent of pH (Figure 5), the acidity/basicity of HE aerosols could be a parameter relevant to S(IV) oxidation rates if subsequent processes were to depend on aerosol pH. 79,80 Therefore, our conclusion that the main pathway for NO2(g) in HEs is reaction R1 will stand regardless of future assessments of aerosol pH. The parameters that may affect a heterogeneous process such as reaction R1 could be a combination of aerosol S/V and aerosol liquid water content, both of which depend on relative humidity.<sup>79,80</sup> We suggest that the apparent dependence of sulfate formation rates on ammonia neutralization of aerosol particles may be the result of cross-correlations between aerosol acidity and the actual causal parameters. In this connection, we point out that the enhancing "ammonium" effect on the rates of oxidation of  $SO_2(g)$  by  $NO_2(g)$  on aqueous solutions might be due to the presence of HSO<sub>4</sub>anions that capture NO<sub>2</sub>(g) at the aerial interface, as explained above.<sup>33</sup> It is also important to realize that the results of Clifton et al.,<sup>54</sup> on the homogeneous reaction rates of HSO<sub>3</sub><sup>-</sup>(aq) with the NO<sub>2</sub>(aq) produced in situ within the bulk solution via NO<sub>2</sub><sup>-</sup>(aq) radiolysis, cannot be applied to the heterogeneous processes being considered here, which involve NO<sub>2</sub>(g) as a

**4.2. HONO** and  $NO_2^-$  as S(IV) Oxidizers. Aqueous HONO and  $NO_2^-$  can oxidize  $HSO_3^-$  to  $HSO_4^-$  in the pH range of 3–5 of HE aerosols. Reductions of HONO and  $NO_2^-$  to NO  $[E^{\circ}(HONO + H^+ + e = NO + H_2O) = 0.75 \text{ V}$ , and

 $E^{\circ}(NO_2^- + 2 H^+ + e = NO + H_2O) = 1.08 V$  or to  $N_2O$  $[E^{\circ}(2HONO + 4H^{+} + 4e = N_{2}O + 3H_{2}O) = 1.06 \text{ V}, \text{ and}]$  $E^{\circ}(2NO_{2}^{-} + 6H^{+} + 4e = N_{2}O + 3H_{2}O) = 1.04 \text{ V}$  could also drive the thermal (dark) oxidation of HSO<sub>3</sub><sup>-</sup> to HSO<sub>4</sub><sup>-</sup>  $[E^{\circ}(HSO_3^- + H_2O = HSO_4^- + 2H^+ + 2e) = 0.15 \text{ V}]$  at pH 4, depending on the concentrations of the reactants and products. The oxidation of HSO<sub>3</sub> by HONO and NO<sub>2</sub>, however, is complex and proceeds slowly via a free radical mechanism through S- and N-containing intermediates. 81-83 In the presence of air, O2 could participate in this process (see below).84

HONO and NO<sub>2</sub><sup>-</sup>, however, could also produce OH radicals at significant rates via photolysis, even in optically thick hazes. Estimates made by using the TUV radiation model show that the photolysis of HONO (from reaction R1) (reaction R3)

$$HONO + h\nu (\lambda \le 390 \text{ nm}) = NO + {}^{\bullet}OH$$
 (R3)

is a stronger and more direct source of OH radicals than the photolysis of  $O_3(g)$  even at the [HONO] =  $0.01[O_3]$  relative abundances measured during HEs.<sup>28</sup> This is due to the much larger solar irradiance in the  $\lambda \leq 390$  nm actinic range compared with that in the  $\lambda \leq 310$  nm range where  $O_3(g)$ dissociates into  $O(^{1}D)$ :  $O_{3} + h\nu = O_{2} + O(^{1}D)$ . Our estimates furthermore suggest that rates of production of OH radicals from HONO during hazy and clear days could be comparable, because faster production and slower HONO photolysis under hazy conditions are offset by slower production and faster HONO photolysis during clear days (Table S1 and Figure S3). We therefore suggest that the production of \*OH via HONO photolysis during HEs could play a significant role in sulfate formation.85

However, because  $pK_2(HONO) \sim 3^{86}$  some N(III) will be also present as  $NO_2^{-1}(aq)$  in the pH range of 3-5. The photolysis of NO2-(aq) also produces OH, but at rates much lower than that of HONO(g), both because of the integrated molar absorptivity of  $NO_2^- \sim 15$  times smaller than that of HONO and because the quantum yield of \*OH production  $[\phi(\mathrm{NO_2^-(aq)} \to {}^{\bullet}\mathrm{OH}) \overset{\frown}{\sim} 0.04]$  is 25 times smaller than  $[\phi(\mathrm{HONO(g)} \to {}^{\bullet}\mathrm{OH}) = 1.0],^{87}$  due to solvent cage effects. Because the reaction of HSO<sub>3</sub><sup>-</sup> with OH from the photolysis of HONO and NO<sub>2</sub><sup>-</sup> and, presumably, also the thermal (dark) reaction between NO2- and HSO3- both proceed via free radicals, O2 is expected to participate in these processes and lead to chain oxidation mechanisms.

The preceding considerations lead us to suggest that  $NO_2(g)$ oxidizes S(IV) indirectly via the free radical mechanism shown below, rather than directly via reaction R0.

$$2NO_2 + H_2O = H^+ + NO_3^- + HONO$$
 (i)

$$HONO + h\nu = NO + {}^{\bullet}OH$$
 (ii)

$${}^{\bullet}\text{OH} + \text{HSO}_{3}^{-} + \text{O}_{2} = \text{HSO}_{4}^{-} + \text{HOO}^{\bullet}$$
 (iii)

$${}^{\bullet}OH + RH + O_2 = RO_x + HOO^{\bullet}$$
 (iv)

$$HOO^{\bullet} + NO = NO_2 + {}^{\bullet}OH$$
 (v)

$$NO_2 + HSO_3^- + O_2 + H_2O$$
  
=  $NO_3^- + HSO_4^- + H^+ + {}^{\bullet}OH$  (R4)

Steps iii and iv as written are not elementary reactions but may proceed via R-OO and H-OO intermediates. The overall stoichiometry of reaction R4 indicates that NO<sub>2</sub> and HSO<sub>3</sub>

produce equimolar amounts of NO<sub>3</sub><sup>-</sup> and HSO<sub>4</sub><sup>-</sup>, plus an OH radical that can oxidize HSO<sub>3</sub><sup>-</sup> as well as other species, RH. If OH reacts with organics RH instead of HSO<sub>3</sub>, the HOO produced in reaction iv will regenerate \*OH via reaction v as long as there is sufficient NO remaining. Therefore, although NO2 may not be the direct oxidizer of SO2 during HEs, the oxidative capacity of the atmosphere will still be determined by the initial NO<sub>2</sub> concentrations. As noted above, a related thermal chain oxidation mechanism may be initiated by  $NO_2^-$ + HSO<sub>3</sub><sup>-</sup>.

**4.3.** Atmospheric Implications. This work focused on the particular heterogeneous chemistry that takes place during the severe wintertime HEs observed in major Chinese cities. We show that the rapid formation of sulfate aerosols during HEs cannot be due to the direct reaction of HSO<sub>3</sub><sup>-</sup> with NO<sub>2</sub>. Instead, S(IV) could be oxidized indirectly by NO2 via the HONO and NO<sub>2</sub><sup>-</sup> produced in its fast hydrolytic disproportionation  $[2NO_2(g) + H_2O(1) = H^+ + NO_3^-(aq) + HONO]$ (reaction R1)], a process that is catalyzed by anions at airaqueous aerosol interfaces. The proposed mechanism naturally accounts for the formation of  $\bar{NO_3}^-$  in the aerosol phase and the significant concentrations of HONO in the gas phase reported by all field studies. It is expected to be favored at the high relative humidity and high S/V aerosol densities that are prevalent during HEs. We show that the photolysis of HONO and NO<sub>2</sub> can be a significant source of OH radicals even under hazy conditions and point out that the thermal reaction between NO<sub>2</sub><sup>-</sup> and HSO<sub>3</sub><sup>-</sup> also proceeds via free radicals, both of which can initiate oxidative chains in the presence of O2. These findings suggest that future field campaigns should focus on OH radical measurements during winter HEs, an issue that has not been properly addressed in the literature. The main insight is that the relevant parameter for a heterogeneous process such as reaction R1 is the surface density S/V of aerosol hazes, which is related to the particle size distribution, and the fluidity of the interfacial layers, rather than to the acidity of aerosol particles. The apparent dependence of sulfate formation rates on ammonia neutralization of aerosol particles may be the result of cross correlations between aerosol acidity and the actual causal parameters. Whereas it remains true that the oxidation of SO<sub>2</sub> during HEs is driven by primary NO<sub>2</sub> emissions, our work, by clarifying the actual mechanism by which this process is initiated, could guide future research efforts and help optimize future air pollution control strategies.

In summary, the direct reaction of NO<sub>2</sub>(g) with HSO<sub>3</sub><sup>-</sup> on the surface of aqueous aerosols is insignificant in the pH range of 3-6. On the surface of aqueous electrolyte solutions, such as those of HE aerosols, NO<sub>2</sub>(g) is mainly converted to NO<sub>3</sub><sup>-</sup> and HONO/NO<sub>2</sub> via hydrolytic disproportionation. The implication is that the oxidation of HSO<sub>3</sub><sup>-</sup> during HEs could be mostly due to thermal (dark)<sup>88</sup> and/or photochemical reactions initiated by HONO/NO<sub>2</sub><sup>-</sup>. The acidity/basicity of HE aerosols could be a parameter relevant to S(IV) oxidation rates only if such processes were to depend on aerosol pH.

## ASSOCIATED CONTENT

## Supporting Information

The Supporting Information is available free of charge on the ACS Publications website at DOI: 10.1021/acs.est.7b05222.

> Figures S1-S4, explanatory note (section S0), TUV calculations (section S1), estimated rates of HONO and OH production (section S2), and Table S1 (PDF)

#### AUTHOR INFORMATION

## **Corresponding Author**

\*E-mail: ajcoluss@caltech.edu.

ORCID 0

Agustín J. Colussi: 0000-0002-3400-4101

Notes

The authors declare no competing financial interest.

## ■ ACKNOWLEDGMENTS

The authors acknowledge financial support from the National Science Foundation (Grants AC-1238977 and AGS-1744353).

#### REFERENCES

- (1) Ma, J.; Chen, Y.; Wang, W.; Yan, P.; Liu, H.; Yang, S.; Hu, Z.; Lelieveld, J. Strong Air Pollution Causes Widespread Haze-Clouds over China. *J. Geophys. Res.* **2010**, *115*, D18204.
- (2) Zheng, G.; Duan, F.; Su, H.; Ma, Y.; Cheng, Y.; Zheng, B.; Zhang, Q.; Huang, T.; Kimoto, T.; Chang, D.; Pöschl, U.; Cheng, Y. F.; He, K. B. Exploring the Severe Winter Haze in Beijing: The Impact of Synoptic Weather, Regional Transport and Heterogeneous Reactions. *Atmos. Chem. Phys.* **2015**, *15*, 2969–2983.
- (3) Zheng, B.; Zhang, Q.; Zhang, Y.; He, K.; Wang, K.; Zheng, G.; Duan, F.; Ma, Y.; Kimoto, T. Heterogeneous Chemistry: A Mechanism Missing in Current Models to Explain Secondary Inorganic Aerosol Formation During the January 2013 Haze Episode in North China. Atmos. Chem. Phys. 2015, 15, 2031.
- (4) Kulmala, M. China's Choking Cocktail. Nature 2015, 526, 497.
- (5) Fu, H.; Chen, J. Formation, Features and Controlling Strategies of Severe Haze-Fog Pollutions in China. *Sci. Total Environ.* **2017**, *578*, 121–138.
- (6) Lin, M.; Tao, J.; Chan, C.-Y.; Cao, J.-J.; Zhang, Z.-S.; Zhu, L.-H.; Zhang, R.-J. Regression Analyses between Recent Air Quality and Visibility Changes in Megacities at Four Haze Regions in China. *Aerosol Air Qual. Res.* **2012**, *12*, 1049–1061.
- (7) Bouarar, I.; Xuemei, W.; Brasseur, G. P. Air Pollution in Eastern Asia: An Integrated Perspective; Springer: Cham, Switzerland, 2017.
- (8) Xu, P.; Chen, Y.; Ye, X. Haze, Air Pollution, and Health in China. Lancet 2013, 382, 2067.
- (9) Huang, R.-J.; Zhang, Y.; Bozzetti, C.; Ho, K.-F.; Cao, J.-J.; Han, Y.; Daellenbach, K. R.; Slowik, J. G.; Platt, S. M.; Canonaco, F.; et al. High Secondary Aerosol Contribution to Particulate Pollution During Haze Events in China. *Nature* **2014**, *514*, 218–222.
- (10) Gao, J.; Woodward, A.; Vardoulakis, S.; Kovats, S.; Wilkinson, P.; Li, L.; Xu, L.; Li, J.; Yang, J.; Li, J.; Cao, L.; Liu, X.; Wu, H.; Liu, Q. Public Health and Mitigation Measures in China: A Review of the Current Evidence for Further Policy Response. *Sci. Total Environ.* 2017, 578, 148–157.
- (11) Gao, M.; Guttikunda, S. K.; Carmichael, G. R.; Wang, Y.; Liu, Z.; Stanier, C. O.; Saide, P. E.; Yu, M. Health Impacts and Economic Losses Assessment of the 2013 Severe Haze Event in Beijing Area. *Sci. Total Environ.* **2015**, *511*, 553–561.
- (12) Liu, Z.; Xie, Y.; Hu, B.; Wen, T.; Xin, J.; Li, X.; Wang, Y. Size-Resolved Aerosol Water-Soluble Ions During the Summer and Winter Seasons in Beijing: Formation Mechanisms of Secondary Inorganic Aerosols. *Chemosphere* **2017**, *183*, 119–131.
- (13) Guo, S.; Hu, M.; Zamora, M. L.; Peng, J.; Shang, D.; Zheng, J.; Du, Z.; Wu, Z.; Shao, M.; Zeng, L.; Molina, M. J.; Zhang, R. Elucidating Severe Urban Haze Formation in China. *Proc. Natl. Acad. Sci. U. S. A.* **2014**, *111*, 17373–17378.
- (14) Quan, J.; Tie, X.; Zhang, Q.; Liu, Q.; Li, X.; Gao, Y.; Zhao, D. Characteristics of Heavy Aerosol Pollution During the 2012–2013 Winter in Beijing, China. *Atmos. Environ.* **2014**, *88*, 83–89.
- (15) Wang, Y.; Zhang, Q.; Jiang, J.; Zhou, W.; Wang, B.; He, K.; Duan, F.; Zhang, Q.; Philip, S.; Xie, Y. Enhanced Sulfate Formation During China's Severe Winter Haze Episode in January 2013 Missing from Current Models. *J. Geophys. Res. Atmos.* **2014**, *119* (10), 10425–10440.

- (16) Li, G.; Bei, N.; Cao, J.; Huang, R.; Wu, J.; Feng, T.; Wang, Y.; Liu, S.; Zhang, Q.; Tie, X.; Molina, L. T. A Possible Pathway for Rapid Growth of Sulfate During Haze Days in China. *Atmos. Chem. Phys.* **2017**, *17*, 3301–3316.
- (17) Yu, H.; Ren, L.; Kanawade, V. P. New Particle Formation and Growth Mechanisms in Highly Polluted Environments. *Curr. Pollut. Rep.* **2017**, *3*, 245–253.
- (18) Hu, B.; Zhao, X.; Liu, H.; Liu, Z.; Song, T.; Wang, Y.; Tang, L.; Xia, X.; Tang, G.; Ji, D.; Wen, T.; Wang, L.; Sun, Y.; Xin, J. Quantification of the Impact of Aerosol on Broadband Solar Radiation in North China. *Sci. Rep.* **2017**, *7*, 44851.
- (19) Deng, X.; Zhou, X.; Tie, X.; Wu, D.; Li, F.; Tan, H.; Deng, T. Attenuation of Ultraviolet Radiation Reaching the Surface Due to Atmospheric Aerosols in Guangzhou. *Chin. Sci. Bull.* **2012**, *57*, 2759–2766
- (20) Xia, D.; Chen, L.; Chen, H.; Luo, X.; Deng, T. Influence of Atmospheric Relative Humidity on Ultraviolet Flux and Aerosol Direct Radiative Forcing: Observation and Simulation. *Asia-Pacific J. Atmos. Sci.* **2016**, *52*, 341–352.
- (21) Quan, J.; Liu, Q.; Li, X.; Gao, Y.; Jia, X.; Sheng, J.; Liu, Y. Effect of Heterogeneous Aqueous Reactions on the Secondary Formation of Inorganic Aerosols During Haze Events. *Atmos. Environ.* **2015**, *122*, 306–312
- (22) He, H.; Wang, Y.; Ma, Q.; Ma, J.; Chu, B.; Ji, D.; Tang, G.; Liu, C.; Zhang, H.; Hao, J. Mineral Dust and Nox Promote the Conversion of So2 to Sulfate in Heavy Pollution Days. Sci. Rep. 2015, 4, 4172.
- (23) Kulmala, M.; Petäjä, T.; Kerminen, V.-M.; Kujansuu, J.; Ruuskanen, T.; Ding, A.; Nie, W.; Hu, M.; Wang, Z.; Wu, Z.; Wang, L.; Worsnop, D. R. On Secondary New Particle Formation in China. *Front. Environ. Sci. Eng.* **2016**, *10*, 8.
- (24) Che, H.; Xia, X.; Zhu, J.; Li, Z.; Dubovik, O.; Holben, B.; Goloub, P.; Chen, H.; Estelles, V.; Cuevas-Agulló, E.; Blarel, L.; Wang, H.; Zhao, H.; Zhang, X.; Wang, Y.; Sun, J.; Tao, R.; Zhang, X.; Shi, G. Column Aerosol Optical Properties and Aerosol Radiative Forcing During a Serious Haze-Fog Month over North China Plain in 2013 Based on Ground-Based Sunphotometer Measurements. *Atmos. Chem. Phys.* 2014, 14, 2125–2138.
- (25) Che, H. Z.; Xia, X. G.; Zhu, J.; Wang, H.; Wang, Y. Q.; Sun, J. Y.; Zhang, X. Y.; Shi, G. Y. Aerosol Optical Properties under the Condition of Heavy Haze over an Urban Site of Beijing, China. *Environ. Sci. Pollut. Res.* 2015, 22, 1043–1053.
- (26) Chen, W.; Tang, H. Z.; Zhao, H. M.; Yan, L. Analysis of Aerosol Properties in Beijing Based on Ground-Based Sun Photometer and Air Quality Monitoring Observations from 2005 to 2014. *Remote Sensing* **2016**, *8*, 110.
- (27) Chen, W.; Yan, L.; Ding, N.; Xie, M. D.; Lu, M.; Zhang, F.; Duan, Y. X.; Zong, S. Analysis of Aerosol Radiative Forcing over Beijing under Different Air Quality Conditions Using Ground-Based Sun-Photometers between 2013 and 2015. *Remote Sensing* **2016**, 8, 510.
- (28) Hou, S. Q.; Tong, S. R.; Ge, M. F.; An, J. L. Comparison of Atmospheric Nitrous Acid During Severe Haze and Clean Periods in Beijing, China. *Atmos. Environ.* **2016**, *124*, 199–206.
- (29) Sun, L.; Li, R. B.; Tian, X. P.; Wei, J. Analysis of the Temporal and Spatial Variation of Aerosols in the Beijing-Tianjin-Hebei Region with a 1 Km Aod Product. *Aerosol Air Qual. Res.* **2017**, *17*, 923–935.
- (30) Zhang, Y.; Huang, W.; Cai, T. Q.; Fang, D. Q.; Wang, Y. Q.; Song, J.; Hu, M.; Zhang, Y. X. Concentrations and Chemical Compositions of Fine Particles (PM2.5) During Haze and Non-Haze Days in Beijing. *Atmos. Res.* **2016**, 174–175, 62–69.
- (31) Lee, Y. N.; Schwartz, S. E. Kinetics of Oxidation of Aqueous Sulfur(IV) by Nitrogen Dioxide. In *Precipitation Scavenging, Dry Deposition and Resuspension*; Pruppacher, H. R., Semonin, R. G., Slinn, W. G. N., Eds.; Elsevier: New York, 1983; Vol. 1, pp 453–466.
- (32) Cheng, Y.; Zheng, G.; Wei, C.; Mu, Q.; Zheng, B.; Wang, Z.; Gao, M.; Zhang, Q.; He, K.; Carmichael, G.; Pöschl, U.; Su, H. Reactive Nitrogen Chemistry in Aerosol Water as a Source of Sulfate During Haze Events in China. *Sci. Adv.* **2016**, *2*, e1601530.

- (33) Wang, G.; Zhang, R.; Gomez, M. E.; Yang, L.; Levy Zamora, M. L.; Hu, M.; Lin, Y.; Peng, J.; Guo, S.; Meng, J.; et al. Persistent Sulfate Formation from London Fog to Chinese Haze. *Proc. Natl. Acad. Sci. U. S. A.* **2016**, *113*, 13630–13635.
- (34) Lammel, G.; Cape, J. N. Nitrous Acid and Nitrite in the Atmosphere. Chem. Soc. Rev. 1996, 25, 361–369.
- (35) Bambauer, A.; Brantner, B.; Paige, M.; Novakov, T. Laboratory Study of NO<sub>2</sub> Reaction with Dispersed and Bulk Liquid Water. *Atmos. Environ.* **1994**, *28*, 3225–3232.
- (36) Cheung, J. L.; Li, Y. Q.; Boniface, J.; Shi, Q.; Davidovits, P.; Worsnop, D. R.; Jayne, J. T.; Kolb, C. E. Heterogeneous Interactions of NO<sub>2</sub> with Aqueous Surfaces. *J. Phys. Chem. A* **2000**, *104*, 2655–2662.
- (37) Lee, Y. N.; Schwartz, S. E. Reaction-Kinetics of Nitrogen-Dioxide with Liquid Water at Low Partial-Pressure. *J. Phys. Chem.* **1981**, 85, 840–848.
- (38) Mertes, S.; Wahner, A. Uptake of Nitrogen-Dioxide and Nitrous-Acid on Aqueous Surfaces. *J. Phys. Chem.* **1995**, *99*, 14000–14006
- (39) Novakov, T. Laboratory Study of NO<sub>2</sub> Reaction with Dispersed and Bulk Liquid Water Reply. Atmos. Environ. 1995, 29, 2559–2560.
- (40) Ponche, J. L.; George, C.; Mirabel, P. Mass-Transfer at the Air-Water-Interface Mass Accommodation Coefficients of SO<sub>2</sub>, HNO<sub>3</sub>, NO<sub>2</sub> and NH<sub>3</sub>. *J. Atmos. Chem.* **1993**, *16*, 1–21.
- (41) Schwartz, S. E.; Lee, Y. N. Laboratory Study of NO<sub>2</sub> Reaction with Dispersed and Bulk Liquid Water. *Atmos. Environ.* **1995**, 29, 2557–2559.
- (42) Colussi, A. J.; Enami, S.; Yabushita, A.; Hoffmann, M. R.; Liu, W. G.; Mishra, H.; Goddard, W. A., III Tropospheric Aerosol as a Reactive Intermediate. *Faraday Discuss.* **2013**, *165*, 407–420.
- (43) Enami, S.; Hoffmann, M. R.; Colussi, A. Absorption of Inhaled NO<sub>2</sub>. *J. Phys. Chem. B* **2009**, *113*, 7977–7981.
- (44) Kinugawa, T.; Enami, S.; Yabushita, A.; Kawasaki, M.; Hoffmann, M. R.; Colussi, A. J. Conversion of Gaseous Nitrogen Dioxide to Nitrate and Nitrite on Aqueous Surfactants. *Phys. Chem. Chem. Phys.* **2011**, *13*, 5144–5149.
- (45) Yabushita, A.; Enami, S.; Sakamoto, Y.; Kawasaki, M.; Hoffmann, M. R.; Colussi, A. J. Anion-Catalyzed Dissolution of NO<sub>2</sub> on Aqueous Microdroplets. *J. Phys. Chem. A* **2009**, *113*, 4844–4848.
- (46) Liu, M.; Song, Y.; Zhou, T.; Xu, Z.; Yan, C.; Zheng, M.; Wu, Z.; Hu, M.; Wu, Y.; Zhu, T. Fine Particle Ph During Severe Haze Episodes in Northern China. *Geophys. Res. Lett.* **2017**, *44*, 5213–5221.
- (47) Shi, G.; Xu, J.; Peng, X.; Xiao, Z.; Chen, K.; Tian, Y.; Guan, X.; Feng, Y.; Yu, H.; Nenes, A.; Russell, A. G. pH of Aerosols in a Polluted Atmosphere: Source Contributions to Highly Acidic Aerosol. *Environ. Sci. Technol.* **2017**, *51*, 4289–4296.
- (48) Weber, R. J.; Guo, H.; Russell, A. G.; Nenes, A. High Aerosol Acidity Despite Declining Atmospheric Sulfate Concentrations over the Past 15 Years. *Nat. Geosci.* **2016**, *9*, 282–285.
- (49) Guo, H.; Nenes, A.; Weber, R. J. The Underappreciated Role of Nonvolatile Cations on Aerosol Ammonium-Sulfate Molar Ratios. *Atmos. Chem. Phys. Discuss.* **2017**, 1.
- (50) Guo, H.; Weber, R. J.; Nenes, A. High Levels of Ammonia Do Not Raise Fine Particle pH Sufficiently to Yield Nitrogen Oxide-Dominated Sulfate Production. *Sci. Rep.* **2017**, *7*, 12109.
- (51) He, K.; Zhao, Q.; Ma, Y.; Duan, F.; Yang, F.; Shi, Z.; Chen, G. Spatial and Seasonal Variability of PM2.5 Acidity at Two Chinese Megacities: Insights into the Formation of Secondary Inorganic Aerosols. *Atmos. Chem. Phys.* **2012**, *12*, 1377.
- (52) Xiyuan, C.; Pengzhen, H.; Zhuang Jiang, X. Y.; Fange, Y.; Longquan, W. Aerosol Acidity During Winter Heavy Haze Episodes in Beijing and Gucheng, China. *Kisho-cho Kenkyu Jiho* **2018**, 32, n/a.
- (53) Lee, Y. N.; Schwartz, S. E. Reaction-Kinetics of Nitrogen-Dioxide with Liquid Water at Low Partial-Pressure. *J. Phys. Chem.* **1981**, 85, 840–848.
- (54) Clifton, C. L.; Altstein, N.; Huie, R. E. Rate Constant for the Reaction of Nitrogen Dioxide with Sulfur (IV) over the pH Range 5.3–13. *Environ. Sci. Technol.* **1988**, 22, 586–589.

- (55) Enami, S.; Colussi, A. J. Criegee Chemistry on Aqueous Organic Surfaces. *J. Phys. Chem. Lett.* **2017**, *8*, 1615–1623.
- (56) Enami, S.; Hoffmann, M. R.; Colussi, A. J. Acidity Enhances the Formation of a Persistent Ozonide at Aqueous Ascorbate/Ozone Gas Interfaces. *Proc. Natl. Acad. Sci. U. S. A.* **2008**, *105*, 7365–7369.
- (57) Enami, S.; Hoffmann, M. R.; Colussi, A. J. Absorption of Inhaled NO<sub>2</sub>. *J. Phys. Chem. B* **2009**, *113*, 7977–7981.
- (58) Enami, S.; Hoffmann, M. R.; Colussi, A. J. Proton Availability at the Air/Water Interface. J. Phys. Chem. Lett. 2010, 1, 1599–1604.
- (59) Enami, S.; Hoffmann, M. R.; Colussi, A. J. OH-Radical Specific Addition to Glutathione S-Atom at the Air-Water Interface: Relevance to the Redox Balance of the Lung Epithelial Lining Fluid. *J. Phys. Chem. Lett.* **2015**, *6*, 3935–3943.
- (60) Enami, S.; Sakamoto, Y.; Colussi, A. J. Fenton Chemistry at Aqueous Interfaces. *Proc. Natl. Acad. Sci. U. S. A.* **2014**, *111*, 623–628.
- (61) Enami, S.; Vecitis, C. D.; Cheng, J.; Hoffmann, M. R.; Colussi, A. J. Electrospray Mass Spectrometric Detection of Products and Short-Lived Intermediates in Aqueous Aerosol Microdroplets Exposed to a Reactive Gas. J. Phys. Chem. A 2007, 111, 13032–13037.
- (62) Enami, S.; Hoffmann, M. R.; Colussi, A. J. Molecular Control of Reactive Gas Uptake "on Water". J. Phys. Chem. A 2010, 114, 5817–5822
- (63) Enami, S.; Mishra, H.; Hoffmann, M. R.; Colussi, A. J. Hofmeister Effects in Micromolar Electrolyte Solutions. *J. Chem. Phys.* **2012**, *136*, 154707.
- (64) Enami, S.; Vecitis, C. D.; Cheng, J.; Hoffmann, M. R.; Colussi, A. J. Mass Spectrometry of Interfacial Layers During Fast Aqueous Aerosol/Ozone Gas Reactions of Atmospheric Interest. *Chem. Phys. Lett.* **2008**, 455, 316–320.
- (65) Enami, S.; Stewart, L. A.; Hoffmann, M. R.; Colussi, A. J. Superacid Chemistry on Mildly Acidic Water. *J. Phys. Chem. Lett.* **2010**, 1, 3488–3493.
- (66) Enami, S.; Colussi, A. J. Long-Range Specific Ion-Ion Interactions in Hydrogen-Bonded Liquid Films. *J. Chem. Phys.* **2013**, 138, 184706.
- (67) Wennberg, P. O. Atmospheric Chemistry: Radicals Follow the Sun. *Nature* **2006**, 442, 145–146.
- (68) Hung, H. M.; Hoffmann, M. R. Oxidation of Gas-Phase  $SO_2$  on the Surfaces of Acidic Microdroplets: Implications for Sulfate and Sulfate Radical Anion Formation in the Atmospheric Liquid Phase. *Environ. Sci. Technol.* **2015**, *49*, 13768–13776.
- (69) Fang, T.; Guo, H. Y.; Zeng, L. H.; Verma, V.; Nenes, A.; Weber, R. J. Highly Acidic Ambient Particles, Soluble Metals, and Oxidative Potential: A Link between Sulfate and Aerosol Toxicity. *Environ. Sci. Technol.* **2017**, *51*, 2611–2620.
- (70) Martin, L.; Hill, M.; Tai, A.; Good, T. The Iron Catalyzed Oxidation of Sulfur (IV) in Aqueous Solution: Differing Effects of Organics at High and Low pH. *J. Geophys. Res.* **1991**, *96*, 3085–3097.
- (71) Liu, Y.; Wu, Z.; Wang, Y.; Xiao, Y.; Gu, F.; Zheng, J.; Tan, T.; Shang, D.; Wu, Y.; Zeng, L.; Hu, M.; Bateman, A. P.; Martin, S. T. Submicrometer Particles Are in the Liquid State During Heavy Haze Episodes in the Urban Atmosphere of Beijing, China. *Environ. Sci. Technol. Lett.* 2017, 4, 427–432.
- (72) Huang, R. J.; et al. Concentration and Sources of Atmospheric Nitrous Acid (HONO) at an Urban Site in Western China. *Sci. Total Environ.* **2017**, *593*–*594*, 165–172.
- (73) Li, X.; et al. Exploring the Atmospheric Chemistry of Nitrous Acid (HONO) at a Rural Site in Southern China. *Atmos. Chem. Phys.* **2012**, *12*, 1497–1513.
- (74) Li, Y.; An, J.; Kajino, M.; Li, J.; Qu, Y. Impacts of Additional HONO Sources on Concentrations and Deposition of NOy in the Beijing-Tianjin-Hebei Region of China. *SOLA* **2015**, *11*, 36–42.
- (75) Liu, Z.; Wang, Y. H.; Costabile, F.; Amoroso, A.; Zhao, C.; Huey, L. G.; Stickel, R.; Liao, J.; Zhu, T. Evidence of Aerosols as a Media for Rapid Daytime HONO Production over China. *Environ. Sci. Technol.* **2014**, *48*, 14386–14391.
- (76) Sörgel, M.; Regelin, E.; Bozem, H.; Diesch, J.-M.; Drewnick, F.; Fischer, H.; Harder, H.; Held, A.; Hosaynali-Beygi, Z.; Martinez, M.; Zetzsch, C. Quantification of the Unknown HONO Daytime Source

- and Its Relation to  $NO_2$ . Atmos. Chem. Phys. Discuss. **2011**, 11, 15119–15155.
- (77) Tang, Y.; An, J.; Wang, F.; Li, Y.; Qu, Y.; Chen, Y.; Lin, J. Impacts of an Unknown Daytime Hono Source on the Mixing Ratio and Budget of HONO, and Hydroxyl, Hydroperoxyl, and Organic Peroxy Radicals, in the Coastal Regions of China. *Atmos. Chem. Phys.* **2015**, *15*, 9381–9398.
- (78) Wang, L. W.; et al. Hono and Its Potential Source Particulate Nitrite at an Urban Site in North China During the Cold Season. *Sci. Total Environ.* **2015**, 538, 93–101.
- (79) Bian, Y.; Zhao, C.; Ma, N.; Chen, J.; Xu, W. A Study of Aerosol Liquid Water Content Based on Hygroscopicity Measurements at High Relative Humidity in the North China Plain. *Atmos. Chem. Phys.* **2014**, *14*, 6417–6426.
- (80) Tan, H.; Cai, M.; Fan, Q.; Liu, L.; Li, F.; Chan, P.; Deng, X.; Wu, D. An Analysis of Aerosol Liquid Water Content and Related Impact Factors in Pearl River Delta. *Sci. Total Environ.* **2017**, *579*, 1822–1830.
- (81) Martin, L. R.; Damschen, D. E.; Judeikis, H. S. The Reactions of Nitrogen Oxides with  $SO_2$  in Aqueous Aerosols. *Atmos. Environ.* (1967-1989) **1981**, 15, 191–195.
- (82) Mendiara, S.; Ghibaudi, E.; Perissinotti, L.; Colussi, A. Free Radicals and Diradicals in the Reaction between Nitrous Acid and Bisulfite in Acid Aqueous Media. *J. Phys. Chem.* **1992**, *96*, 8089–8091.
- (83) Littlejohn, D.; Wang, Y.; Chang, S. G. Oxidation of Aqueous Sulfite Ion by Nitrogen Dioxide. *Environ. Sci. Technol.* **1993**, 27, 2162–2167.
- (84) Oblath, S.; Markowitz, S.; Novakov, T.; Chang, S. Kinetics of the Initial Reaction of Nitrite Ion in Bisulfite Solutions. *J. Phys. Chem.* **1982**, *86*, 4853–4857.
- (85) Li, Y.; An, J.; Gultepe, I. Effects of Additional HONO Sources on Visibility over the North China Plain. *Adv. Atmos. Sci.* **2014**, *31*, 1221.
- (86) Riordan, E.; Minogue, N.; Healy, D.; O'Driscol, P.; Sodeau, J. R. Spectroscopic and Optimization Modeling Study of Nitrous Acid in Aqueous Solution. *J. Phys. Chem. A* **2005**, *109*, 779–786.
- (87) Chu, L.; Anastasio, C. Temperature and Wavelength Dependence of Nitrite Photolysis in Frozen and Aqueous Solutions. *Environ. Sci. Technol.* **2007**, *41*, 3626–3632.
- (88) Pires, M.; Rossi, M. J. The Heterogeneous Formation of N<sub>2</sub>O in the Presence of Acidic Solutions: Experiments and Modelling, Regarding the Heterogeneous Oxidation of SO<sub>2</sub> by HONO on Water. *Int. J. Chem. Kinet.* **1997**, 29, 869–891.